Materials Today Bio 32 (2025) 101765

Contents lists available at ScienceDirect

Materials Today Bio

journal homepage: www.journals.elsevier.com/materials-today-bio

Organoid in droplet: Production of uniform pancreatic cancer organoids from single cells

Haitao Liu [a,1], Tingting Tao [a,1], Zhongqiao Gan [a,b], Yingying Xie [a,b], Yaqing Wang [c,d], Yizhao Yang [e], Xu Zhang [a], Xianliang Li [f,*], Jianhua Qin [a,b,c,d,g,**]

[a] Division of Biotechnology, Dalian Institute of Chemical Physics, Chinese Academy of Sciences, Dalian, 116023, China
[b] University of Chinese Academy of Sciences, Beijing, 100049, China
[c] University of Science and Technology of China, Hefei, 230026, China
[d] Suzhou Institute for Advanced Research, University of Science and Technology of China, Suzhou, 215123, China
[e] Imperial College London, White City Campus, London, W12 0BZ, UK
[f] Department of HBP Surgery, Beijing Chao Yang Hospital, the Capital Medical University, Beijing, 100020, China
[g] Beijing Institute for Stem Cell and Regenerative Medicine, Beijing, 100101, China

ARTICLE INFO

Keywords:
Pancreatic cancer
Uniform organoids
Droplet microfluidic
Defined microgels
Drug testing

ABSTRACT

Cancer organoids have improved our understanding of recapitulating the histology, genotypes, and drug response of patient tumors for personalized medicine. However, the existing cancer organoids are typically grown in animal-derived matrices (e.g., Matrigel), which suffer from poor reproducibility and low throughput due to uncontrollable origin of seed cells, undefined matrix, and manual manipulation. Here, we report a new strategy to massively generate uniform pancreatic cancer organoids (PCOs) in a droplet system from single cells. This system is composed of all-in-water fluids that allow to mildly encapsulate single tumor cell into isolated droplet, which subsequently proliferate and self-assemble into organoids, resembling the initial state of a tumor in the body. This high-throughput method can produce thousands of organoids in a single batch. The droplets can serve as templates for synthesizing defined microgels with proper stiffness similar to that of native tumors, facilitating functional expressions of PCOs. These organoids exhibit superior uniformity and controllability in terms of size and morphologies compared with organoids cultured in manually dropped Matrigel, due mainly to the controllable number of initiating cells and defined microgels. In addition, the established organoids maintain the key biomarkers of pancreatic tumor (e.g., KRT7, KRT19 and SOX9) and higher expression of genes associated with drug metabolism confirmed by RNA-seq and PCR analysis. Furthermore, they show distinguishing responses to four clinically used drugs in a reproducible manner in automatic pipetting workstation, indicating the feasibility of the proposed method in high-throughput drug testing. The established strategy has integrated the formation, 3D cultures, and analysis of PCOs derived from single cells in a whole system, which may provide a novel platform for advancing organoids research with standardized procedure in translational applications.

1. Introduction

Patient-derived organoids have emerged as a preferred model for predicting cancer treatments, as they can be generated from tumor biopsy within one month and maintain the histopathological and genomic profiles of the patients [1,2]. These organoids retain tumor tissue heterogeneity and responses to drugs, making them valuable for high-throughput drug screening [3]. Generally, organoids have many advantages over traditional 2D cultures, as they display near-physiological cellular composition and behaviors. Many organoid cultures can undergo extensive expansion in culture and maintain genome stability, which makes them suitable for biobanking [4–6]. Compared to patient-derived xenografts and animal models, organoids can reduce experimental complexity, facilitate precision genetic and imaging techniques, and, more importantly, enable the study of human development and diseases that is not feasible in animals [7–9]. A

* Corresponding author.
** Corresponding author. Division of Biotechnology, Dalian Institute of Chemical Physics, Chinese Academy of Sciences, Dalian, 116023, China.
E-mail address: jhqin@dicp.ac.cn (J. Qin).
[1] These authors contribute equally.

https://doi.org/10.1016/j.mtbio.2025.101765
Received 23 January 2025; Received in revised form 6 April 2025; Accepted 11 April 2025
Available online 12 April 2025

prominent example is pancreatic cancer, a leading cause of cancer-related mortality worldwide with a 5-year survival rate of 12 %, the lowest among recorded tumors [10]. This cancer presents various subtypes, complex etiologies, and diverse patient responses to therapies, posing significant challenges for effective treatment. Moreover, pancreatic cancer often remains asymptomatic until reaching advanced stages due to the pancreas' deep abdominal location. Therefore, the development of preclinical tumor models with high fidelity has garnered considerable attention for advancing research into pancreatic cancer pathogenesis and developing effective diagnostic and therapeutic strategies. In this milieu, pancreatic cancer organoids (PCOs) were generated in 2013 by activating WNT signaling and expressing LGR5 in mouse pancreatic duct fragments [11]. Since then, PCOs have been extensively utilized to replicate tumor progression, evaluate novel anticancer drugs, and promote precision medicine approaches for pancreatic cancer [12–14].

Despite their potential as valuable models of cancer biology, PCOs exhibit several limitations that hinder their reproducibility, throughput, and clinical translation. Typically, the initial number and condition of seeded cells cannot be precisely controlled in the traditional tumor organoids, leading to the random development of organoids. In addition, to support the generation and 3D culture, pancreatic cancer fragments or cells are usually encapsulated in murine Engelbreth-Holm-Swarm (EHS) matrix (e.g., Matrigel) by manual manipulation. Although such matrices can provide a rich milieu of tumor-derived extracellular matrix (ECM) components, growth factors and cytokines, they exhibit remarkable batch-to-batch variability and contain xenogenic impurities that can unpredictably influence organoid phenotype [15]. Furthermore, the Matrigel, with relatively low stiffness (typically less than 1 kPa), fails to reconstruct biophysical microenvironment of pancreatic cancers that showed a Young's modulus of 4~6 kPa or even higher [16–18]. Also, the manual manipulation of PCOs increases the demand of primary tumor tissues for organoids establishment and limits the compatibility of organoids in rapid and high-throughput drug screening.

Recently, droplet microfluidics have been explored to tumor organoid field, usually in terms of organoid culture, formation and drug testing. The combination of organoids and droplet microfluidics partially addressed the challenges of existing PCOs, such as realizing high-throughput generation and manipulation of organoids, and controlling the components and morphology of organoids ECM. By adding prepolymers and patient-derived cells into droplets, various microgels can be produced to form tumor organoids after cellular proliferation and

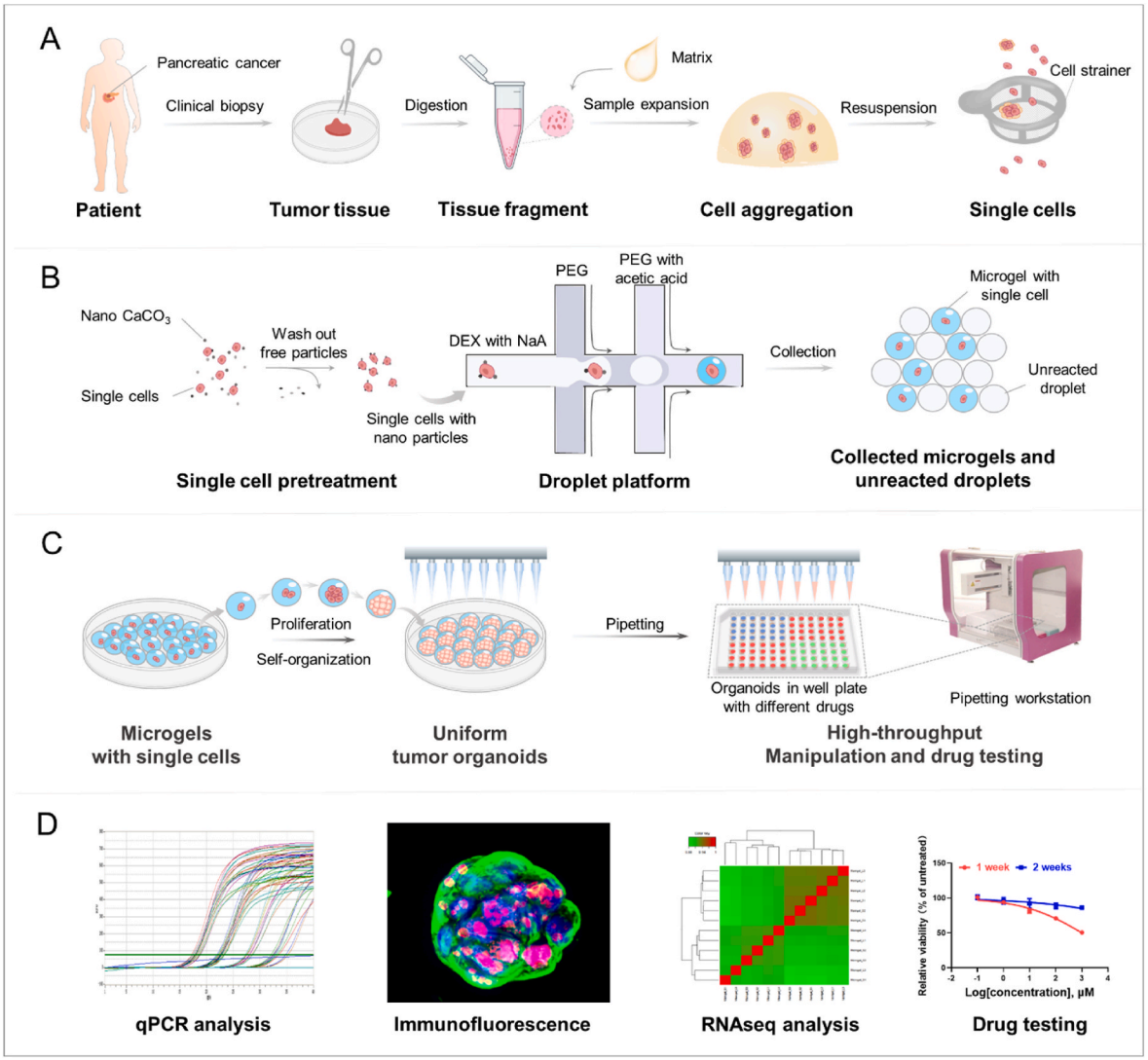

Fig. 1. Schematic diagram of droplet system for rapid generation of uniform PCOs from single cells. (A). The process of collecting dispersed single cells from clinical biopsy. **(B).** The droplet system to effectively encapsulate single tumor cells. **(C).** The 3D culture, manipulation, and high-throughput drug testing of the encapsulated homogeneous PCOs developed from single cells. **(D).** The output data acquired by using the loaded organoids, including PCR, immunofluorescence, RNAseq, and drug testing, etc.

self-organization [19–24]. These organoids have been used for chemotherapy [19,22] and immune therapy [21] testing to show their potential in precision medicine. Nevertheless, the existing technologies often fail to control the initial number of cells in each droplet. This have led to significant variation of the generated organoids, or even generation of more than one organoid in each droplet, which need to be addressed in this filed. Traditionally, alginate hydrogels were used as 3D cell scaffolds in tissue engineering due to their flexibility and biocompatibility that allowed the survival and growth of cells [25]. In addition, alginate is well suited for droplet microfluidics because of its fast and mild cross-linking progress triggered by divalent cationic ions (e.g. Ca^{2+}) [26]. Also, alginate was reported to be used for precisely encapsulating one single cell in each microgel produced in droplet microfluidic device [27], which holds great potential in increasing the controllability and uniformity of the existing tumor organoids.

Here, we provide a new strategy for scalable generation of uniform PCOs in a droplet system from single tumor cells. The clinical biopsies are dissociated and filtered for the construction of PCOs (Fig. 1A). These organoids, derived from single cells, are cultured in defined microgels composed of alginate matrices with tailored stiffness, facilitating high-throughput organoid production and manipulation (Fig. 1B and C). The utilization of single cells would enhance the controllability of seeded cell numbers, and replicate the initial state of a tumor in the body. The developed strategy effectively increases the uniformity of organoids in terms of their size and morphologies and decreases the number of cells demanded for organoids establishment. We systematically characterize the expression of tumor-related biomarkers and genes in organoids by using immunofluorescence and qPCR, comparing them with organoids cultured in Matrigel or primary tumor tissues. We also investigate and validate differential gene expression of PCOs through RNA-seq analysis (Fig. 1D). Finally, we employ PCOs in high-throughput anti-cancer drug testing with automatic pipetting workstation, demonstrating the feasibility of the proposed strategy for preclinical applications.

2. Materials and methods

2.1. Establishment of the droplet system

The multi-layered microfluidic chip was fabricated using standard soft lithography and micromolding approaches. Briefly, the polydimethylsiloxane (PDMS, Dow Corning Corporation, 02085925) at a weight ratio of 10 : 1 was molded from a photoresist (SU-8 3035, MicroChem Corporation, Y311074) templates after being cured at 80 °C for 2 h in an oven to form structured top and middle layers of the chip. Subsequently, the top layer was bonded to the middle layer that was bonded to a plain PDMS block after punching with a diameter punch of 1.5 mm and oxygen plasma treatment. The height and width of the microchannels in top layer are both 300 μm, while the height and width of the microchannels in middle layer are both 100 μm. In addition, the thickness and diameter of pneumatic valve are 200 μm and 1 mm, respectively, which could control the generation of droplet templates.

2.2. Cell culture

Human pancreatic cancer cell lines, 1.1B4 and Panc-1, were purchased from Meisen Chinese Tissue Culture Collections and Shanghai Zhong Qiao Xin Zhou Biotechnology Co.,Ltd, respectively. These cells were cultured using Dulbecco's Modified Eagle Medium (DMEM, high glucose, Gibco, 11965092) supplemented with 10 % fetal bovine serum (FBS, Gibco, 16170078) and 1 % streptomycin and penicillin (Sigma-Aldrich, P0781). They were cultured in a humidified incubator composed of 5 % CO_2 at 37 °C and passaged until achieved 80 %~90 % confluence.

2.3. Human samples

Pancreatic cancer surgical samples were collected at the First Affiliated Hospital of Dalian Medical University after informed patient consent under a protocol approved by the Ethics Committee of the First Affiliated Hospital of Dalian Medical University (Approval number: PJ-KS-KY-2023-162).

2.4. PCOs culture

PCOs were established from resected pancreatic cancer surgical samples and protocols were followed by a previous report [28] after modification. Briefly, tumor tissue was minced and digested with collagenase II (5 mg/mL, Sigma, 1148090) in human complete medium (see below) at 37 °C for 1 h on an orbital shaker. For conventional organoid formation, passage, and conservation, the collected cells were directly embedded in pure Matrigel (Corning, 354230) drops (30 μL/drop) and seeded on 6-well culture plates (Corning, 353046). For the subsequent encapsulation of single cells in microgels, the collected cells were embedded in pure Na-alginate (NaA, 50 kDa, Pharmaceutical grade) solution (1 % (w/v) NaA dissolved in physiological saline) and dropped into 1 % (w/v) $CaCl_2$ (Aladdin, C118704) to form alginate hydrogels (30 μL/drop). Here, the NaA was customized from Qingdao Hyzlin Biology Development Co., Ltd (http://www.hyzlin.com/), which was screened with 80 mesh and its viscosity was 55 cps at the concentration of 1 % (w/v). The physiological saline was prepared by dissolved NaCl (Tianjin Damao Chemical Reagent, analytically pure, 20200908) in water at the concentration of 0.9 % (w/v). Then, the cells were culture with complete medium containing 50 % AdDMEM/F12 medium (Thermo Fisher Scientific, 12634010), Glutamax (1x, Gibco, 35050061), B27 (1x, Gibco, 10889038), R-spondin 1 (100 ng/mL, R&D, AF4645), Noggin (100 ng/mL, R&D, 6057-NG), Wnt3a condition medium (1x, MBL, J2-001), N-acetyl-L-cysteine (1 mM, Sigma, A9165), Nicotinamide (10 mM, Sigma, N0636), epidermal growth factor (EGF, 50 ng/mL, Peprotech, GMP100-15), fibroblast growth factor 10 (FGF10, 100 ng/mL, Prepotech, 100-26), and A83-01 (0.5 μM, Selleck, S769201). The cells formed organoids within 1~2 weeks to remove cells other than tumor cells, such as immune cells, fibroblasts, or other cells by starvation in the complete medium before single cell encapsulation. For passage, organoids within Matrigel drops were first resuspended in the culture plates by using a pipette before transformed to the centrifuge tube and centrifuged for 10 min at 1500 rpm (Eppendorf, 5804). Then, the precipitate was digested with TrypLE (Gibco, 12605010) and resuspended with AdDMEM/F12 medium before centrifuged for 10 min at 1500 rpm. Finally, the digested cells and clusters were embedded in pure Matrigel drops and seeded on 6-well culture plates for the next culture using the complete medium. Organoids within alginate hydrogels were first digested with alginate lyase (Sigma, A1603) at a concentration of 10 U/mL for 10 min to remove the hydrogels before transformed to the centrifuge tube and centrifuged for 5 min at 1500 rpm. Then, the precipitate was digested with TrypLE and resuspended with AdDMEM/F12 medium before centrifuged for 5 min at 1500 rpm. Finally, the digested cells and clusters were embedded in pure alginate drops and seeded on 6-well culture plates for the next culture using the complete medium.

2.5. Pretreatment of single cells before encapsulation

Pancreatic cell lines and the formed PCOs within alginate hydrogels were dissociated by 0.25 % trypsin-EDTA (Gibco, 25200056) and TrypLE, respectively, then filtered into isolated cells using cell strainer (Falcon, 352340) and treated with $CaCO_3$ nanoparticles (40–80 nm, XFNANO, XFI11-1) according to the previous report [27] with minor modification. Briefly, $CaCO_3$ nanoparticles were suspended in $CaCl_2$-free DMEM medium (Gibco, 21068028) at a concentration of 20 mg/mL, which was treated with ultrasound using an ultrasonic cell disruptor

(SCIENTZ-IID, SCENTZ) and filtered to remove the free nanoparticles with a 0.22 μm syringe filter (Millex Syringe Filter, SLGPR33RB) and obtain $CaCO_3$ saturated DMEM (named "DMEM-Ca"). Then, 20 mg/mL $CaCO_3$ suspension was prepared using DMEM-Ca after ultrasonic treatment. Next, the cell suspension was washed with DMEM-Ca by centrifugation at 200×*g* for 3 min and resuspended with DMEM-Ca at a concentration of 2×10^6 cells/mL, which was mixed with 20 mg/mL $CaCO_3$ suspension at a ratio of 1:1. The mixture of cells and $CaCO_3$ was incubated for 15 min at cell culture condition on a shaker before centrifuged at 40×*g* for 5 min. The cells loaded with $CaCO_3$ were washed with DMEM-Ca and centrifuged at 40×*g* for twice to remove the free $CaCO_3$. The pre-treated cells were resuspended in core flow solution with a density of 2.5×10^5 cells/mL for encapsulation experiments.

2.6. Encapsulation of single cells using microgels

The core flow solution was prepared by mixing cell suspensions with a concentrated NaA solution (22.5 % (w/v) dextran (DEX) (500 kDa, GE, 17-0320-02) and 1.5 % (w/v) NaA dissolved in physiological saline) at a ratio of 1:2. The final solution contained 15 % (w/v) DEX and 1 % (w/v) NaA. And 15 % (w/v) polyethylene glycol (PEG) (20 kDa, Aladdin, P103730) and 15 % (w/v) PEG with 0.4 % (v/v) acetic acid (Aladdin, A298827) were also dissolved in physiological saline as the middle and shell flow, respectively. All these solutions were filtered with a 0.22 μm syringe filter before being pumped into the microfluidic chip device. The core, middle and shell flows were pumped into their inlets of the pneumatic valve-integrated chip by using pressure pumps (FLOW-EZ, Fluigent, Beijing E-Science Co., Ltd). In this microfluidic system, the pneumatic valve was pulled periodically as the constant negative pressure (−60 kPa) was connected and unconnected under the control of external solenoid valve, thus leading to a droplet templates generation at the end of a switch cycle at the first junction of chip. Then, droplet templates were delivered into shell flow by middle flow at the second junction, wherein the Ca^{2+} of $CaCO_3$ was released by contacting to the acetic acid, and electrostatic complexation of NaA and Ca^{2+} occurred to form microgels. The generated cell-laden microgels were collected in physiological saline/culture medium before further gelation with 1 % (w/v) $CaCl_2$ for 10 min. The cells in microgels were finally transferred to cell culture medium within a 96-well culture plate (Corning, 3474) and cultured in a humidified incubator with 5 % CO_2 at 37 °C with the fresh medium being changed every other day. As control group, the formed PCOs within Matrigel were digested with TrypLE and filtered to be isolated cells, resuspended in pure Matrigel drops (30 μL/drop), and seeded on 6-well culture plates at the concentration of 2.5×10^5 cells/mL. Then, the culture plates were placed upside down in a humidified incubator with 5 % CO_2 at 37 °C to keep the morphology of dome Matrigel drops that were solidified after 30 min. Finally, culture medium was added in the culture plates with the fresh medium being changed every other day.

2.7. Diameter measurement of microgels and organoids

The implementation of size measurement of microgels and organoids are using Image J software (http://rsb.info.nih.gov/ij/). Specifically, the long axis and short axis of microgels/organoids are manually measured using the optical images, and the average of long axis and short axis is used as the diameter of the given microgels/organoids.

2.8. Young's modulus measurement of microgels

The microgels fabricated using different concentrations (0.5 %, 1 % and 2 %) of NaA were collected and fixed at the bottom of confocal dish (Biosharp, BS-20-GJM) coated with 1 % (w/v) chitosan (100–200 cps, Aladdin, C105799) that was dissolved in water with pH = 5 adjusted by acetic acid. Then, the Young's modulus of microgels were measured by using a Piuma Nanoindenter (Optics11) with a probe of appropriate range. Each sample was measured at least in triplicate. Finally, the primary tumor tissues and Matrigel were also tested on their Young's modulus for comparation with that of the produced microgels.

2.9. Scanning electron microscope (SEM) analysis of microgels

Hydrous microgels were freeze-dried in a lyophilizer (SCIENTZ-10ND, China) for at least 4 h. Then the microgels were coated with a layer of gold for 60 s with a sputter coater (SBC-12, KYKY) at the electricity of 8 mA. The size and surface morphology of the microgels were characterized using a SEM (Hitachi TM3000, Japan) at 15 kV. To investigate the internal structure of microgels, the core flow solution without cells was manually dropped into a collection tank of 1 % (w/v) $CaCl_2$ to form large microgels that were dissected before SEM analysis. In addition, pure NaA solution (1 % (w/v) NaA dissolved in physiological saline) was prepared and dropped into 1 % (w/v) $CaCl_2$ to form pure alginate hydrogels and Matrigel was dropped into empty culture plates for gelation at 37 °C, respectively. Here, the pure alginate hydrogels and Matrigel were used as control groups to microgels. The implementation of porosity/sectional area of pore measurement of microgels, Matrigel and pure alginate hydrogels are using Image J software (http://rsb.info.nih.gov/ij/).

2.10. Endotoxin testing of core flow solution with different concentrations of NaA

The content of endotoxin in core flow solution with different concentrations of NaA was tested by using endotoxin assay kit (GenScript, L00350C). Core flow solutions with 15 % DEX and varied NaA, including 0.5 %, 1 %, 2 % and 3 %, were prepared and the endotoxin was tested according to the user's manual, and the absorbance at 545 nm was measured with a microplate reader (Tecan Infinite M Nano).

2.11. Live/dead testing of encapsulated cells

The proportion of viable cells within microgels was evaluated by using live/dead assay. The cell-laden microgels were incubated in cell culture medium with ethidium homodimer-1 (red, dead, 1:500) and calcein-AM (green, live, 1:1000) (LIVE/DEAD viability/cytotoxicity assay kit, Gibco, L3224) at 37 °C for 25 min. Then, they were rinsed with physiological saline before imaging under a laser scanning confocal microscope (FV3000, Olympus). The viability percentage was determined by counting the number of live cells (green fluorescence), which was divided by the total number of live (green fluorescence) and dead (red fluorescence) cells at a given focal plane. In addition, the viability percentage of cells before encapsulation was measured using the same method.

2.12. Fluorescence immunohistochemistry of organoids

Pancreatic cell spheroids and PCOs in microgels, as well as PCOs in Matrigel were soaked in 4 % paraformaldehyde (PFA) (MeilunBio, MA0192) for 20 min at room temperature to be immobilized after cultivation of 10 days. Then, they were permeabilized with 0.2 % Triton X-100 (Amresco, SH11087) for 10–15 min and blocked in a blocking solution (ZSGB-BIO, ZLI-9022) for 1 h at room temperature, successively. Next, these cells were incubated at 4 °C overnight with the required primary antibodies that are listed in the supplementary information (Table S1), which were diluted with antibody diluent (ZSGB-BIO, ZLI-9028) in the experiment. Then, the second antibodies of IgG H&L (Alexa Fluor®, ab150077, ab150080, ab150113, and ab150116, Abcam) were used to treat the aforesaid cells at a dilution rate of 1:500 for 2 h at room temperature. The cell nuclei were stained with DAPI (1:4000, CST 4083) for 15 min at room temperature. All the images were acquired with the laser scanning confocal microscope.

2.13. Real-time quantitative PCR (qPCR)

The whole mRNA was extracted from PCOs in microgels and Matrigel with the Trizol reagent (TAKARA, 9109) after alginate lyase treatment and mechanical stirring, respectively, to detect the associated genes expression level. The whole mRNA was also extracted from primary tumor tissues with the Trizol reagent after mechanical lapping and used as the reference for PCOs in microgels and Matrigel. The final concentration of mRNA was adjusted to 50 ng/mL. The cDNA was then synthesized by reverse transcription polymerase chain reaction (RT-PCR) using a reverse transcription kit (TAKARA, RR037A). Subsequently, real-time quantitative PCR was implemented with a SYBR Green kit (TAKARA, RR820) under the following reaction conditions (40 cycles): denaturation at 95 °C for 30 s, annealing at 58 °C for 30 s, and extension at 72 °C for 30 s. The primer pairs were synthesized by Sangon Biotech and listed in the supplementary information (Table S2). Quantification was performed using GAPDH as the reference gene.

2.14. RNA-seq analysis of PCOs

The PCOs cultured in microgels and Matrigel drops (1 week and 2 weeks) were treated with alginate lyase and mechanical stirring, respectively, for cell retrieval and the mRNA was extracted using the Trizol reagent according to the supplier's information. For each sample, 500 ng total RNAs were used for stranded RNA sequencing library preparation using KC-Digital Stranded mRNA Library Prep Kit for Illumina (Catalog No. DR08502, Wuhan SeqHealth Co., Ltd., China) following the manufacturer's instruction. An average of 49 million reads per sample was uniquely aligned to the hg38 human reference genome (GRCh38) STAR software (version 2.5.3a) with default parameters. The kit eliminates duplication bias in PCR and sequencing steps, using unique molecular identifier (UMI) of eight random bases to label the preamplified cDNA molecules. The library products corresponding to 200–500 bps was enriched, quantified, and finally sequenced on Hiseq X 10 sequencer (Illumina). Alternative splicing events were detected using rMATS (version 3.2.5) with an FDR value cutoff of 0.05 and an absolute value of $\Delta\psi$ of 0.05. Gene Ontology (GO) and Kyoto Encyclopedia of Genes and Genomes (KEGG) enrichment analysis for differentially expressed genes was implemented by KOBAS software (version: 2.1.1) with a corrected P-value cutoff of 0.05 to judge whether it has statistically significant enrichment. The RNA-seq data reported in this paper were accessible in the SRA with the accession code PRJNA1110825.

2.15. Anti-tumor drug testing of PCOs

PCOs grown in microgels for 1 week and 2 weeks were exposed to 4 selected compounds for a further 24 h to test the cell viability. Briefly, approximately 200 organoids in each single well of a 96-well plate containing 200 μL culture media were added with Gemcitabine (MeilunBio, MB5386), Erlotinib (MeilunBio, MB1734-1), Olaparib (MeilunBio, MB1700), and 5-Fluorouracil (MeilunBio, MB1273) at 6 concentrations of 0, 0.1, 1, 10, 100, and 1000 μM in the automatic pipetting workstation (TIANGEN, AP400). As the frequency of generating single-cell-laden microgels can be precisely controlled by the pneumatic valve (the reciprocal of valve period is the generation frequency of microgels), the number of organoids for drug testing can also be controlled. Then, the resulting organoids was incubated using a cell counting kit-8 (CCK-8, MeilunBio, MA0225) assay according to the user's manual, and the absorbance at 450 nm was measured with a microplate reader. Here, the viability of organoids treated by drugs at the concentration of zero was set as 100 % viability, and the other viability was normalized by the 100 % viability. In a separate experiment, the resulting organoids that were treated by drugs were labeled with Ki67 and TUNEL Apoptosis Assay Kit (Elabscience, E-CK-A321) according to the manufacturer's protocol, respectively, to validate the proliferation and apoptosis of organoids. All the images were acquired with the laser scanning confocal microscope.

2.16. Statistic

In this work, all experiments were performed at least in triplicate. The PCR data were presented as mean ± Standard Error of the Mean, others were presented as mean ± Standard Deviation. The ΔΔCt method was used for PCR data. Statistical significance was declared when $*p < 0.05$, $**p < 0.01$ and $***p < 0.001$ as determined by one-way ANOVA and student's t-test.

3. Results

3.1. Development of droplet system for the generation of PCOs from single cells

Current tumor organoids are limited by their variation partially due to the uncontrollable origin of each organoid and undefined physicochemical properties of matrices. To improve the uniformity of the resulting tumor organoids, we set up a droplet system to synthesize PCOs within defined microgels from single tumor cells. The droplet system was constructed according to our previous study [29,30]. We used a multilayered and valve-integrated microfluidic chip (Figs. S1A and S1C) to fabricate the defined alginate microgels in all-in-water fluids. DEX solution with NaA and PEG solution were utilized as core and middle flows that pumped into the chip, respectively, for the formation of droplet templates. Since alginate has been previously used as 3D cell scaffolds in tissue engineering due to their flexibility and biocompatibility [25], we chose it as the matrix of organoids. In addition, alginate is well suited for droplet microfluidics because of its fast and mild cross-linking mechanism [26], as well as holds great potential in precisely encapsulating one single cell in each microgel [27], which lines with our needs in this work. The single tumor cells derived from clinical biopsy or the formed PCOs were mixed in the core flow after attached with $CaCO_3$ nanoparticles that can release Ca^{2+} once contacting the acetic acid in the shell flow for the gelation of NaA to form Ca-alginate (CaA) microgels within the chip (Fig. 2A). Then, the unloaded droplets were filtered out by gently wash, and effective encapsulation of single cells can be realized. In this system, the negative pressure driven by a solenoid valve controller was utilized to activate the normally closed pneumatic valve for controlling the generation manners of droplet templates (Fig. S1B). Herein, we used PEG solution as the continuous phase to establish the all-in-water microfluidic system, instead of using traditional oil phase (e.g., mineral oil). In this system, although the throughput of droplets decreased slightly, we directly obtained cell-laden microgels by using the pretreated cells without additional demulsification step (e.g., adding demulsifier and using vigorous centrifugation). Also, the all-in-water system increased the biocompatibility of the progress of producing cell-laden microgels. All of these would ensure the cell viability within microgels after encapsulation.

The microgels serve as an engineered niche crucial for the formation and 3D culture of PCOs, ensuring consistent size and morphology for a stable microenvironment. In the droplet system, the rates of all the pumped flows are key parameters that affect the dimensional and structural properties of the produced microgels. Thus, we first measured the average diameter, and the ratio of long to short axis (L/S) of microgels that generated under serial rates of core flow. As shown in Fig. 2B and D, the diameter of microgels increases with the core flow rate significantly, which is commonsensible in droplet microfluidic system due to the correlation between dispersed phase flow rate and droplet size within certain range [31]. In addition, the value of L/S is also positively related to the core flow rate (Fig. 2D). However, no remarkable variations caused by changing middle/shell flow rates on the diameter or L/S value of microgels were observed (data not shown). This might be because of the little contribution of middle/shell flows to the formation of droplet templates in our system. Since the droplet

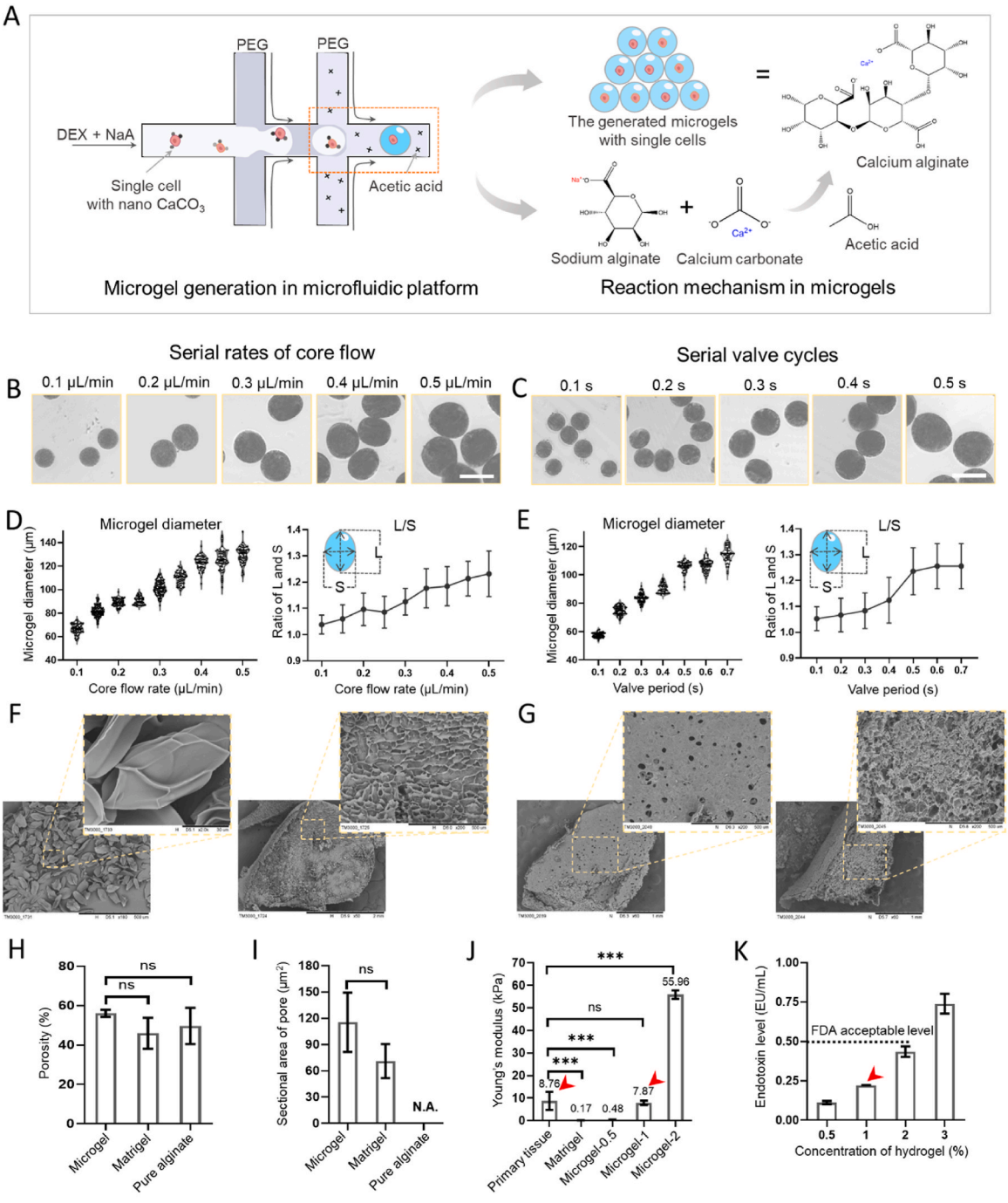

Fig. 2. The characterization of defined microgels. (A). Schematic diagram of the massive and controllable generation of microgels with single cells. **(B).** Microgels generated under serial rates of core flow, ranging from 0.1 to 0.5 μL/min. Scale bar: 100 μm. **(C).** Microgels generated under serial valve cycles, ranging from 0.1 to 0.7 s. Scale bar: 100 μm. **(D).** Microgel diameter as a function of core flow rate, as well as the ratio of long and short axis of microgels (L/S) as a function of core flow rate. **(E).** Microgel diameter as a function of valve cycle, as well as the ratio of long and short axis of microgels (L/S) as a function of valve cycle. Quantitative analysis of the diameter of microgels were performed on at least 50 microgels. **(F).** SEM images of intact microgels and cross section of microgels. The scale bars in the images are 500 μm, 30 μm, 2 mm, and 500 μm from left to right. **(G).** SEM images of the surface and cross section of Matrigel dome. The scale bars in the images are 1 mm, 500 μm, 1 mm, and 500 μm from left to right. **(H).** The porosity of freeze-dried microgels, Matrigel and pure alginate hydrogels. **(I).** The average sectional area of pore within freeze-dried microgels, Matrigel and pure alginate hydrogels, which represents the pore size of corresponding matrices. **(J).** Young's modulus of primary tumor tissues, Matrigel, and microgels fabricated with different concentrations of alginate. Microgel-0.5, microgel-1, and microgel-2 represent microgels fabricated with 0.5 %, 1 %, and 2 % NaA, respectively. **(K).** Determination of endotoxin contamination of the alginate prepolymers with different concentrations. FDA acceptable level was indicated with dotted blue line (0.5 EU/mL). Statistical significance was declared when $*p < 0.05$, $**p < 0.01$ and $***p < 0.001$ as determined by student's t-test for Fig. 2H, I and 2J. (For interpretation of the references to color in this figure legend, the reader is referred to the Web version of this article.)

generation manner is highly controlled by the pneumatic valve (Movie S1), we also investigated the microgels generated under different valve periods that were defined as the total time of a switch cycle from valve being pulled to relaxed. In this milieu, we found that the valve periods exhibited the same influence as core flow rates on the microgels (Fig. 2C and E), further indicating the apparent shape and size of microgels can be precisely modulated. In addition, a microgel is produced during each valve period, and the microgel yield is 85–600/min when the valve period is 0.1s–0.7s. And the size distribution analysis of microgels generated under different experimental parameters revealed low polydispersity, with a relatively small coefficient of variation (CV < 7 %, data not shown).

3.2. *Characterization of the defined microgels generated from droplet system for organoids culture*

Before the 3D culture of PCOs, we evaluated several fundamental characteristics of alginate microgels. SEM analysis of freeze-dried microgels showed smooth surface and typical porous structures (Fig. 2F). It is worth noting that we directly dropped the core flow solution to the shell flow solution to obtain microgels with large volume for easy observation of the internal structures. Correspondingly, we investigated the surficial and sectional morphologies of Matrigel and pure alginate hydrogels as well at the same conditions. Although the true pore size and porosity of these matrices at cell culture condition cannot be analyzed with these freeze-dried ones, we can provide

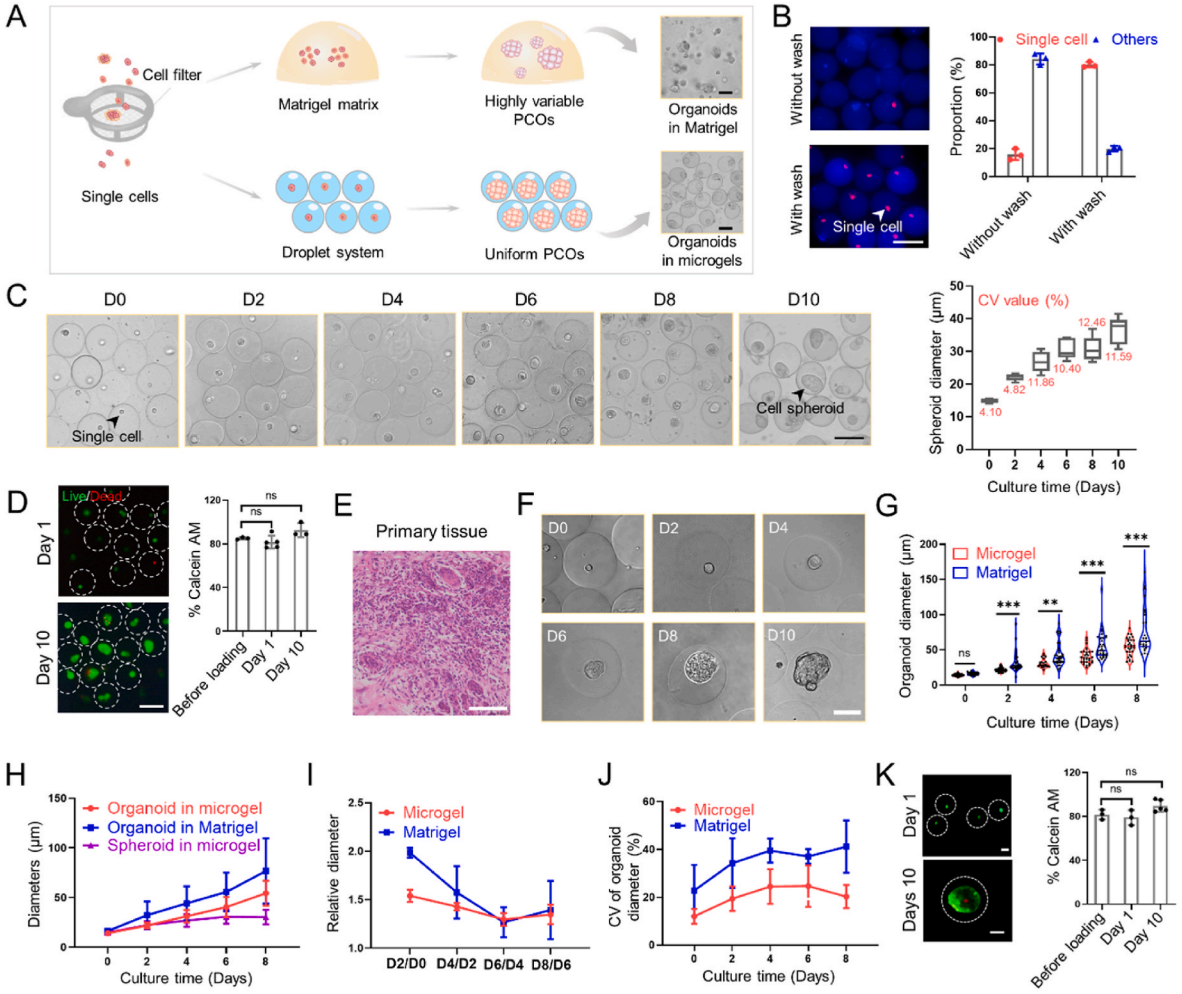

Fig. 3. The formation of PCOs in defined microgels from single cells. (A). Schematic diagram of the scalable generation of PCOs from single cells. **(B).** Monodisperse 1.1B4 cells encapsulated in microgels using droplet platform with/without washing unadsorbed $CaCO_3$ nanoparticles, and the percentage of single-cell-laden microgels (single-cell-laden microgels relative to the total number of the produced microgels). Here, total number of the produced microgels includes the number of single-cell-laden microgels, multiple-cells-laden microgels, and microgels without cells. In the image, "Single cell" means single-cell-laden microgels, and "Other" means the summation of multiple-cells-laden microgels and microgels without cells. **(C).** Representative images and growth of 1.1B4 cell spheroids in microgels after encapsulation in 0~10 days. The average diameters of spheroids at days 0, 2, 4, 6, 8, and 10 were calculated here. **(D).** Cell viability of 1.1B4 cell spheroids in microgels was evaluated at days 1 and 10 of culture by using Live/Dead Kit. The green and red fluorescence represent live and dead cells, respectively. The percentage of live cells before and after encapsulation was calculated here. **(E).** The architecture of primary tumor tissue characterized by H&E. **(F).** Representative images of PCOs after encapsulation in microgels for 0–10 days. **(G).** The growth of PCOs in defined microgels and commercial Matrigel. **(H).** Growth curve of 1.1B4 cell spheroids in microgels, as well as PCOs in microgels and Matrigel. **(I).** Relative diameter of PCOs in microgels and Matrigel for 0–10 days. Here, D2/D0 represent the ratio of organoid diameter at days 2 and day 0, and so on in a similar fashion. **(J).** The dimensional variability of PCOs cultured in microgels and Matrigel. Here, we calculated the CV of organoid diameter in microgel or Matrigel group in triplicate at each time point. The average value of each CV was shown in this figure. **(K).** Cell viability of PCOs was evaluated at days 1 and 10 of culture by using Live/Dead Kit. The green and red fluorescence represent live and dead cells, respectively. The percentage of live cells before and after encapsulation was calculated here. Scale bars are 100 μm for (Ã E), 50 μm for (F and K). Statistical significance was declared when *p < 0.05, **p < 0.01 and ***p < 0.001 as determined by student's t-test in Fig. 3D, G and 3K. (For interpretation of the references to color in this figure legend, the reader is referred to the Web version of this article.)

valuable comparison among them. Compared to Matrigel, microgels exhibited smoother surface (Fig. 2F and G), as well as slightly larger porosity and sectional area of pores (Fig. 2H and I). While microgels and pure alginate hydrogels exhibited similar porosity (Fig. 2H). As for the sectional area of pores, pure alginate hydrogels showed overlarge pore size that could not be measured precisely (Fig. S2). The difference between microgels and pure alginate hydrogels due possibly to the porogen effects of DEX within microgels. The porous structure of microgels, which facilitate the exchange of nutrients and wastes between tumor tissues and the external microenvironment, is crucial for the formation and proliferation of PCOs.

It has been reported that the Young's modulus of pancreatic cancer tissues is 4~6 kPa or even higher [16–18], which is remarkably higher than that of Matrigel (less than 1 kPa). The stiffness of pancreatic cancer is highly involved in tumor progression and phenotype, including their invasion [32], metastasis [33], fibrosis [34], and sensitivity to chemotherapy [16]. Here, we tested the stiffness of microgels generated with different concentrations of NaA to explore their suitability for PCOs culture. As shown in Fig. 2J, pure Matrigel and microgels fabricated with 0.5 %, 1 %, and 2 % alginate (labeled as microgel-0.5, microgel-1, and microgel-2) display growing Young's modulus of 0.17 ± 0.04, 0.48 ± 0.04, 7.87 ± 0.96, 55.95 ± 6.16 kPa, respectively. Also, we measured the stiffness of primary pancreatic cancer tissues as a criterion, of which the Young's modulus was 8.76 ± 3.99 kPa, close to that of microgel-1. Moreover, the endotoxin of core flow solution with different concentrations of NaA was determined to estimate the biocompatibility of proposed microgels for biomedical applications. The results show that the endotoxin level of core flow solution is below the Food and Drug Administration (FDA)-regulated endotoxin levels (0.5 EU/mL) for implantable medical devices when the concentration of NaA is below 2 % (Fig. 2K). This demonstrates the compatibility of droplets and microgels for cell encapsulation and culture.

In the droplet system, the biopsies or formed PCOs were digested and filtered into single cells for the encapsulation using defined microgels (Fig. 3A). To assess the possibility of microgels for encapsulation and culture of single cells, two pancreatic cell lines (1.1B4 and Panc-1) were pretreated with $CaCO_3$ nanoparticles and resuspended in the core flow to produce single-cell-laden microgels. We first directly mixed 1.1B4 cells and $CaCO_3$ nanoparticles in the core flow solution to explore the optimal cell density for effective single-cell loading. The results show that the proportion of empty microgels decreases as cell density increases (Figs. S3A and S3B). The proportion of single-cell-laden microgels show positively related to cell density, and the proportion of multiple-cells laden microgels significantly increases when cell density is greater than 2.5×10^5/mL (Fig. S3B). Therefore, 2.5×10^5 cells/mL might be a proper density for effective single-cell loading. In addition, we compared the efficacy of single-cell-laden microgels formation using pretreated 1.1B4 cells with/without washing unadsorbed $CaCO_3$ nanoparticles at the cell density of 2.5×10^5/mL. As shown in Fig. 3B, the proportion of single-cell-laden microgels (single-cell-laden microgels relative to the total number of the produced microgels) has been improved from 15.8 % to 80.1 % by washing unadsorbed $CaCO_3$ nanoparticles before cell loading. Specifically, cells with adsorbed $CaCO_3$ nanoparticles would be the only sources of Ca^{2+} for NaA gelation within droplets after washing unadsorbed $CaCO_3$ nanoparticles, which means droplets without cells cannot form solid microgels. These unloaded and unreacted droplets would be dissolved into the surrounding medium when transferred or gently washed the cell-laden microgels, thus improving the efficacy of cell-laden microgels formation, of which the single-cell-laden microgels domains at the given cell density.

After encapsulation, the 1.1B4 cells within microgels kept growing and spontaneously formed cellular spheroids with relatively low CV below 13 % during 10 days of culture (Fig. 3C). Moreover, the tumor spheroids showed favorable cell viability demonstrated by live/dead assays over time (Fig. 3D). It is interesting that the proportion of living cells in microgels after 10 days of culture (92.6 %) is higher than that of cells before loading (85.0 %), further indicating that the process of cell loading and niche provided by microgels are biocompatible for living cells. We also evaluated the expression of tumor-related biomarkers to show the potential of encapsulated cell spheroids as *in vitro* tumor models. As shown in Fig. S4A, the expressions of tumor (EpCAM), ductal lineage (KRT19), and proliferation (Ki67) markers confirm the basic properties of pancreatic tumors in 1.1B4 cells. The expressions of MMP1 and Vimentin are related to matrix remodeling and cell migration, indicating the possibility of using these spheroids for tumor invasion research. The similar expressions of tumor-related biomarkers were also observed in the loaded Panc-1 spheroids (Fig. S4B), demonstrating the universality of our methodology for encapsulation and 3D culture of various pancreatic tumor cell lines.

3.3. High-throughput generation of uniform PCOs from single cells

In the following section, we investigated the feasibility of our strategy for the high-throughput generation of uniform PCOs from single cells. The clinical biopsies were initially minced, digested into isolated cells, and used to form PCOs in Matrigel or pure alginate hydrogels, following procedures outlined in previous reports [28] to remove the non-neoplastic cells by starvation in tumor culture medium. In the proposed droplet system, we can obtain up to thousands of organoids in each single experiment. Compared with using multiple cells or cell clusters for constructing tumor organoids, using single cells can increase the controllability of seeded cell numbers. As shown in Fig. 3E, the primary tumor tissues exhibit dense architecture before being used. The pancreatic cancer cells were loaded in microgels in a single-cell manner and gradually grew into cellular spheroids, or called PCOs during 10 days of 3D culture (Fig. 3F). On the contrary, pancreatic cancer cells aggregated spontaneously in Matrigel at the beginning of encapsulation and grew to be organoids with variable size from single cells (Fig. S5). Thus, more organoids can be obtained in the microgels when the initial number of cells is the same in microgels and Matrigel, indicating better formation efficiency of organoids in microgels. It seems that the microgel diameter does not change throughout spheroid/organoid growth (Fig. 3C and F). However, in fact, the diameter of spheroid/organoid is only half that of microgel at days 10. According to the sphere calculation formula ($V = \frac{4}{3}\pi R^3$, where V is the volume of a sphere and R is the radius of the sphere), the spheroid/organoid within microgel would increase the volume of microgel by 12.5 %, and increase its diameter by 4.0 % that is too small to be conscious. In this study, PCOs in Matrigel grow faster than those in microgels, but both can keep proliferation during the culture, shown in Fig. 3G and H. To explore the possible reasons, we calculated the relative diameter (the ratio of organoid diameter at latter time point to previous time point) of PCOs in microgels and Matrigel (termed as Mi-organoids and Ma-organoids). The results showed that the relative diameter, that is growth rate, of Ma-organoids is higher than that of Mi-organoids in the first 4 days. Subsequently, two types organoids showed the similar growth rate possibly due to the adaptive process of pancreatic cancer cells to the single-cell microenvironment in microgels in the first 4 days or the lack of bioactive components of microgels (Fig. 3I). And this leads to the relative slow growth of organoids in microgels in the first 4 days, after which, the cell growth rate was significantly improved. By following the same PCO-laden microgel aligned in a microwell, we investigated the dynamic process of the certain PCOs (Fig. S6). The results showed that the initial location of the single cell did not influence the formation or growth of PCOs significantly, if the cells remained in the microgels. In addition, most of the PCOs (over 70 %) began to migrate outside the microgels by days 9~10 of culture at the given fabrication condition due probably to their increased diameter (over half of that of the microgels) that was not well tolerated by the microgels. As such, we usually measured the diameter of organoids up to day 8, even if they were

cultured for 10 days. But a few single cells that was initially encapsulated at the margin of microgels and migrated outside prematurely, which could not maintain proliferation or form PCOs well without the 3D spatial support from microgels. It is worth noting that patient-derived pancreatic cancer cells within microgels grow faster than cell lines (Fig. 3H), indicating that the former adapt better to 3D culture condition. This also demonstrates that patient-derived organoids are better choices for rapid establishment of *in vitro* 3D models than cell lines.

The PCOs cultured in defined microgels and Matrigel were also compared on their uniformity over the 10 days of culture. The results show that the dimensional uniformity of Mi-organoids is better than that of Ma-organoids, as evidenced by lower CV of organoid diameter (Fig. 3J), highlighting the remarkable advantage of our approach in improving organoid homogeneity. In addition, the cell viability of PCOs was evaluated by using Live/Dead Kit, shown in Fig. 3K. The process of encapsulation and 3D culture did not decrease the proportion of living cells, demonstrating the proliferative capacity of the organoids in microgels. To verify the tumor-specific features of organoids, we investigated the expression of several biomarkers by using immunofluorescence analysis. The significant expressions of ductal lineage (KRT19) and proliferation (Ki67) markers in Mi-organoids reflect the origin of pancreatic tumor (Fig. 4A). And the expressions of KRT19, KRT7, and Ki67 in Mi-organoids were comparable with that of Ma-organoids (Fig. 4B and S7). Also, the expressions of KRT19 and Ki67 of Mi-organoids were significantly higher than those of spheroids composed of cell lines (Fig. S4), further demonstrating that patient-derived organoids are better on reflecting tumor features than cell lines. Since these organoids all exhibited dense structures, the defined microgels were also used for encapsulation and formation of PCOs with

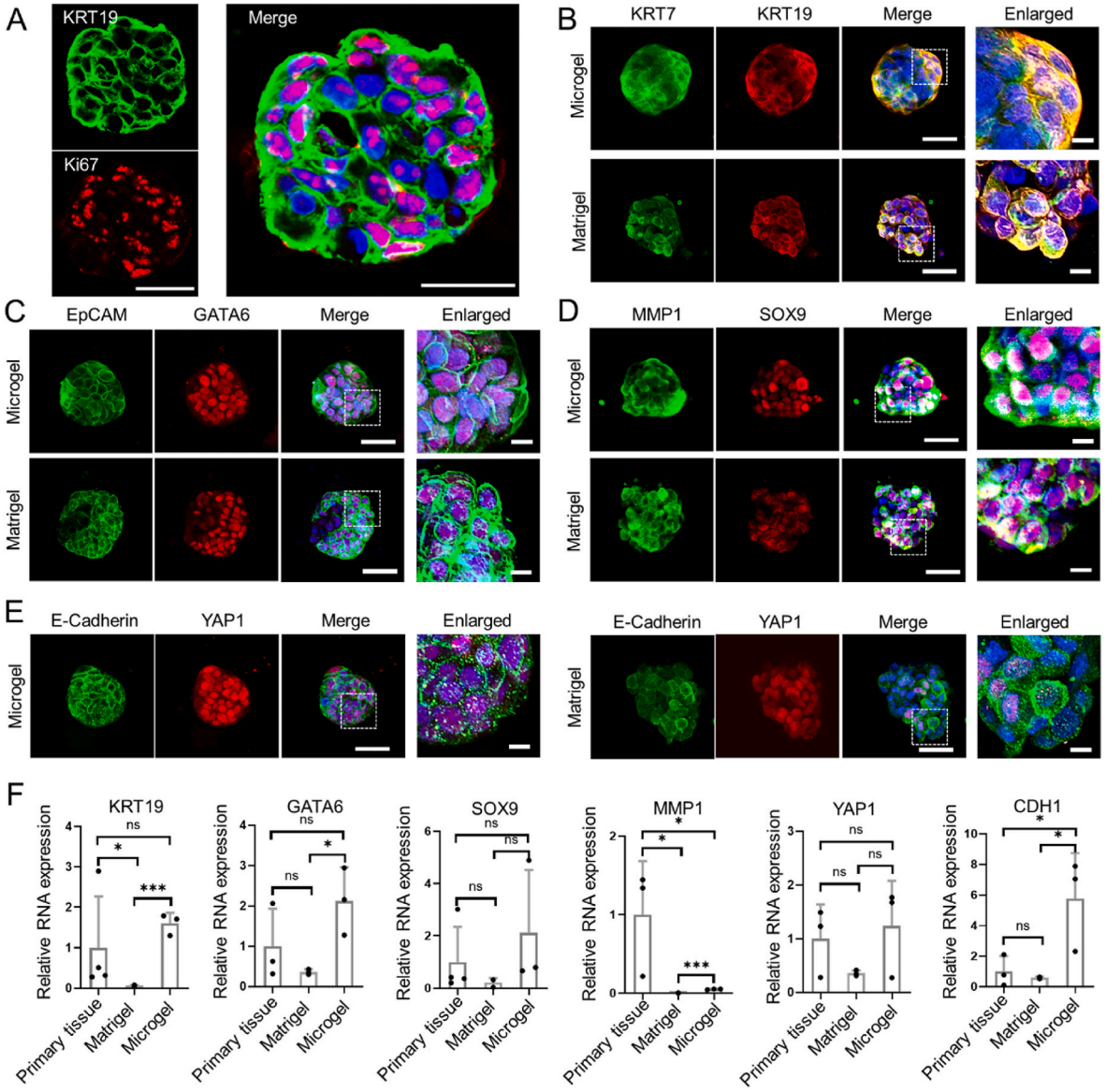

Fig. 4. Identification of formation and functions of PCOs in defined microgels. (A). Immunohistochemical staining of specific proteins (KRT19 and Ki67) in pancreatic tumors after 10 days of encapsulation in microgels. Scale bars: 50 μm. Immunohistochemical staining of cancer markers: **(B).** KRT19 and KRT7, **(C).** EpCAM and GATA6, **(D).** MMP1 and SOX9, **(E).** E-cadherin and YAP1 in PCOs after 10 days of encapsulation in microgels and Matrigel. DAPI stained the nuclei (blue). Scale bars: 50 μm for unenlarged images and 10 μm for enlarged images. **(F).** The expressions of tumor-associated genes (KRT19, GATA6, SOX19, MMP1, YAP1, and CDH1) are examined on primary tumor tissues, as well as cancer organoids cultured in microgels and Matrigel using qPCR. Statistical significance was declared when *$p < 0.05$, **$p < 0.01$ and ***$p < 0.001$ as determined by student's t-test. (For interpretation of the references to color in this figure legend, the reader is referred to the Web version of this article.)

typical acinar structures at the conditions described in Section 2.4-2.6 from the patients with alternative tumor phenotype to demonstrate the universality of our approach (Fig. S8). The expressions of typical tumor markers (e.g. KRT7, KRT19, Vimentin and EpCAM) in acinar PCOs proved the reproducibility of the proposed method across patient tumor samples.

Furthermore, endodermal (GATA6) and ductal lineage (SOX9) markers were significantly expressed in the Mi-organoids (Fig. 4C and D), further confirming their tumor-specific features. The expressions of tumor-related (EpCAM) and invasion-related (MMP1) markers suggests that our PCOs could be used *in vitro* models in the research of tumor progression. The expressions of all the four markers exhibited similar patterns in Mi-organoids and Ma-organoids. However, the Mi-organoids show higher expressions of E-cadherin and YAP1 compared to Ma-organoids (Fig. 4E), indicating tighter connections between cells and more mechanotransduction occur in Mi-organoids probably due to the stiffer matrices composed of CaA. Furthermore, the higher expression of E-cadherin is associated with lower ability of epithelial-mesenchymal transition (EMT), which is dispensable for tumor metastasis but induces chemoresistance in pancreatic cancers [35]. All these biomarkers expressed by cell clusters in microgels also confirmed the formation of tumor organoids. To quantitively evaluate the differences of Mi-organoids and Ma-organoids, as well as determine which one better recapitulated the characteristics of primary tumor tissues, we analyzed these samples by using qPCR. As shown in Fig. 4F, endodermal (GATA6), ductal lineage (KRT19), tumor (CDH1) and tumor invasion (MMP1) associated genes display remarkably higher expression in Mi-organoids compared with Ma-organoids. In addition, the expressions of most of the genes, including KRT19, GATA6, SOX9, YAP1 and CDH1, in primary tumor tissues are higher than those in Ma-organoids, while lower than those in Mi-organoids. In consideration of the existing of non-neoplastic cells within primary tumor tissues, the actual expressions of the above genes of tumor cells within primary tumor tissues should be higher than the displaying ones. Thus, compared to Ma-organoids, Mi-organoids might be better choice to replicate the characteristics of primary tumor tissues.

3.4. Transcriptional analysis of the generated PCOs

To gain an overview of the molecular signatures of PCOs, we analyzed the transcriptional profiles of Mi-organoids and Ma-organoids after two weeks of 3D culture using RNA-seq. The volcano plots show that 2360 genes are differentially expressed in Mi-organoids compared with that in Ma-organoids, among which, 950 genes are upregulated and 1410 genes downregulated (Fig. 5A). All these genes were subjected to hierarchical clustering, showing the unique gene set enriched in Mi-organoids in comparison to that of Ma-organoids ($P < 0.05$, fold change >2) (Fig. 5B). We then used KEGG pathway analysis to estimate the mainly differentiated biological pathways between two organoids and selected all the ones closely related to tumors or pancreas for exhibition. As shown in Fig. 5C, the biological pathways associated with arachidonic acid metabolism, ABC transporters, and linoleic acid metabolism, etc. were upregulated, while the glycolysis/gluconeogenesis, biosynthesis of amino acids, and central carbon metabolism in cancer, etc. were downregulated in Mi-organoids comparison to that of Ma-organoids. Since drug screening is a typical and important

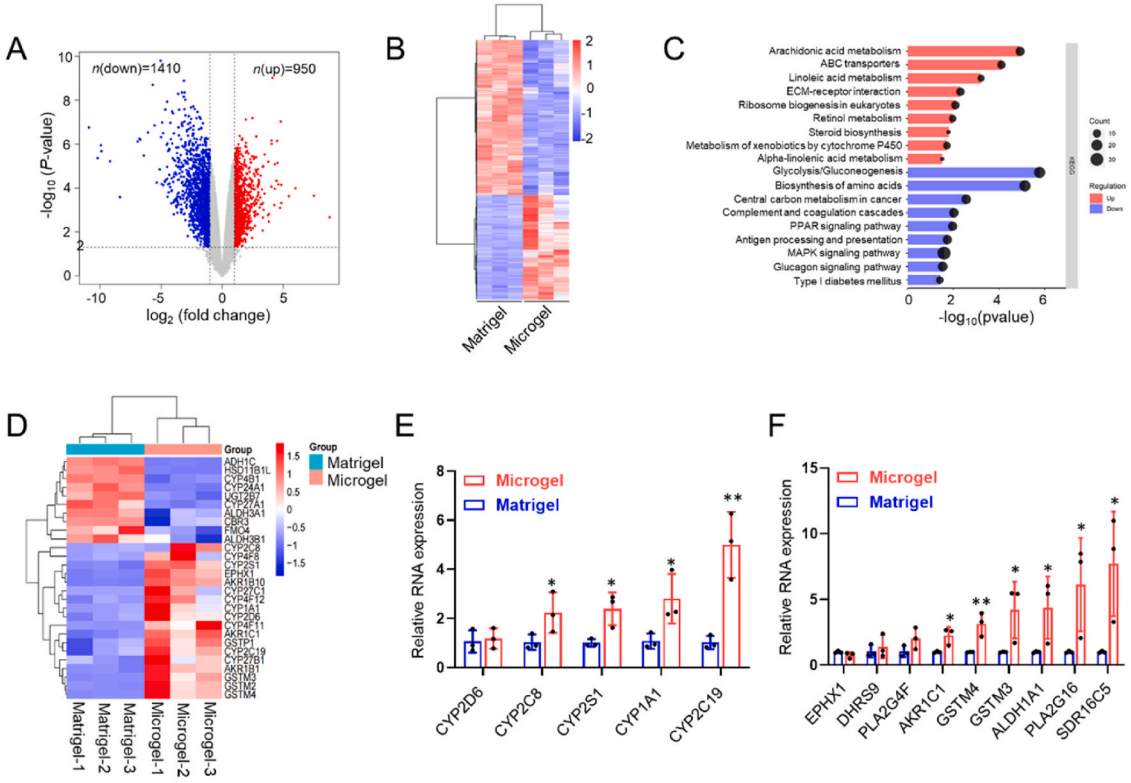

Fig. 5. RNA-seq analysis of PCOs cultured in microgels. (A). Volcano plots of the dysregulated genes of organoids cultured in microgels vs in Matrigel. **(B).** Heat map of the dysregulated genes of organoids cultured in microgels vs in Matrigel. **(C).** The selected KEGG pathway enrichment analysis of differentially expressed genes in cancer organoids cultured in microgels vs in Matrigel. **(D).** Heat map of the dysregulated genes related to drug metabolism of organoids cultured in microgels vs in Matrigel. Genes differentially expressed with a fold change greater than 2.0 and $P < 0.05$ are marked in color. P-values were calculated using a two-sided, unpaired Student's t-test, assuming equal variances (n = 3 independent biological samples). **(E).** and **(F).** Validation of selected DEGs identified by RNA-seq using qRT-PCR. The expression values were normalized to GAPDH. Data were normalized against expression values of organoids cultured in Matrigel and are shown as mean ± SEM, three independent experiments were performed. (For interpretation of the references to color in this figure legend, the reader is referred to the Web version of this article.)

application of PCOs, we selected all the differentially expressed genes involved in drug metabolism and subjected them to a new hierarchical clustering (Fig. 5D). The results showed that 64.29 % of the selected genes were upregulated in Mi-organoids compared to Ma-organoids.

Impressively, biological pathways related to the metabolism of xenobiotics by cytochrome P450 were upregulated in Mi-organoids, suggesting potential implications for drug metabolism in PCOs. To quantify the expression of increased genes of this pathway, qPCR assay was performed (Fig. 5E and F). In Mi-organoids, transcription of genes encoding cytochrome P450 superfamily of enzymes (CYP1A1, CYP2C8, CYP2C19, CYP2S1), Aldo-Keto reductase (AKR1C1), glutathione S-transferase (GSTM3, GSTM4), aldehyde dehydrogenase (ALDH1A1), phospholipase A and acyltransferase (PLA2G16), and short chain dehydrogenase/reductase (SDR16C5), were significantly upregulated. The expression of genes encoding epoxide hydrolase (EPHX1), cytochrome P450 superfamily of enzymes (CYP2D6), dehydrogenase/reductase (DHRS9), and phospholipase (PLA2G4F) exhibited no obvious changes. Previous reports have demonstrated that CYP2S1 is a prognostic prediction in pancreatic cancer [36], and the high expression of CYP2C8 were related to the high mortality of patients [37]. Generally, PLA2G16 and SDR16C5 are upregulated in pancreatic cancer patients [38,39], with increased expression of the SDR16C5 promoting the proliferation

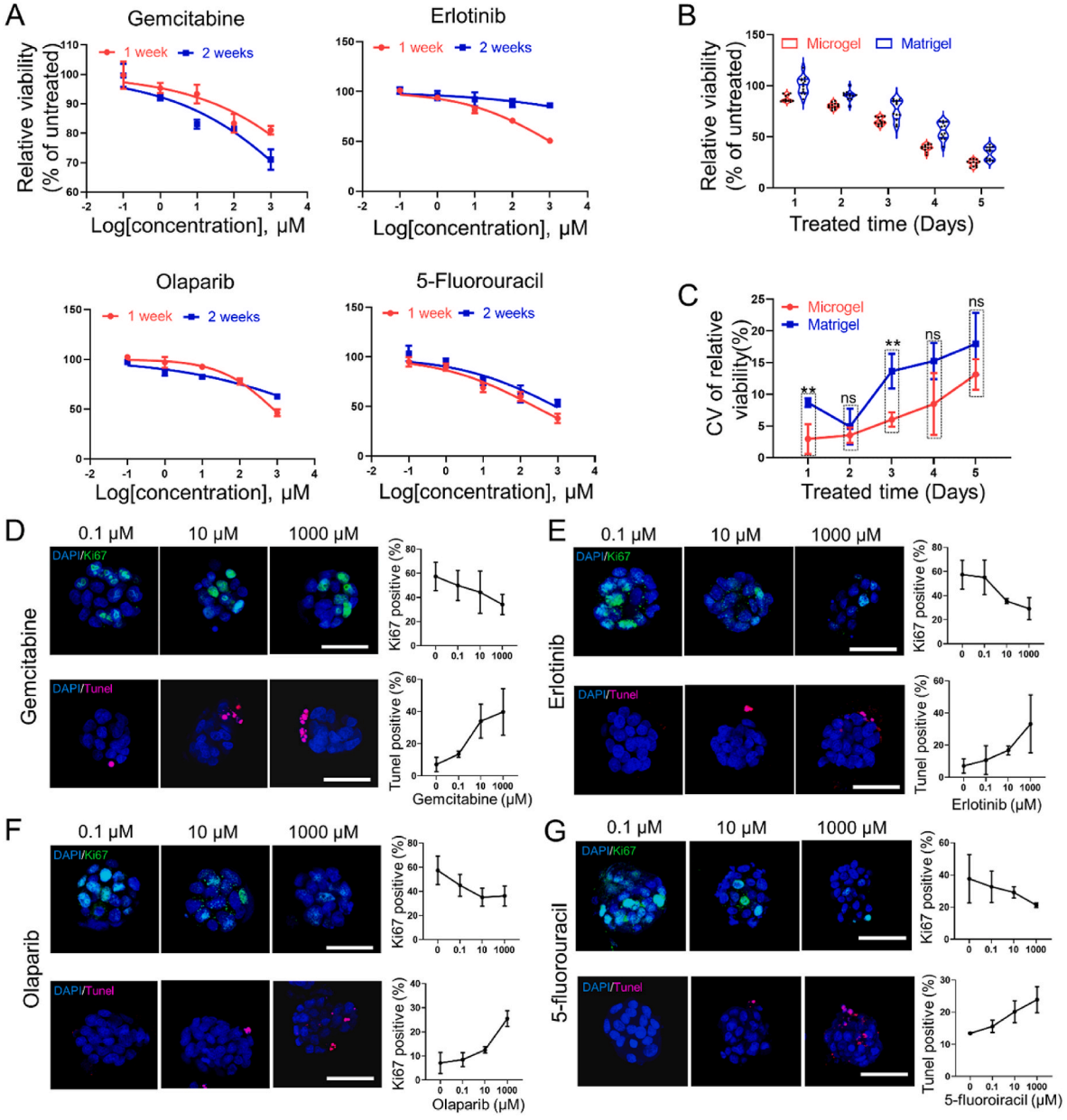

Fig. 6. Tumor chemosensitivity testing in PCOs from single cells. (A). Relative cell viability of organoids cultured in microgels as a function of logarithmic Gemcitabine, Erlotinib, Olaparib and 5-fluorouracil concentration at days 7 and 14. The cell viability organoids is normalized by that of the untreated organoids. **(B).** Relative viability of PCOs cultured in microgel and Matrigel after Erlotinib treatment for 5 days at the concentration of 50 μM. **(C).** The viability variability of PCOs cultured in microgels and Matrigel after Erlotinib treatment for 5 days at the concentration of 50 μM. Here, we calculated the CV of relative cell viability within organoids cultured in microgel or Matrigel group in triplicate at each time point. The average value of each CV was shown in this figure. Statistical significance was declared when *$p < 0.05$, **$p < 0.01$ and ***$p < 0.001$ as determined by student's t-test at each time point between the CV of Mi-organoids and Ma-organoids. **(D).** The proliferation and apoptosis of organoids after Gemcitabine treatment for 24 h at days 7. **(E).** The proliferation and apoptosis of cells within organoids after Erlotinib treatment for 24 h at days 7. **(F).** The proliferation and apoptosis of cells within organoids after Olaparib treatment for 24 h at days 7. **(G).** The proliferation and apoptosis of cells within organoids after 5-fluorouracil treatment for 24 h at days 7. For figures (D)–(G), only Mi-organoids were tested. Scale bars: 50 μm.

and migration of pancreatic cancers while inhibiting their apoptosis [40]. In addition, the high expression of CYP2C19 and ALDH1A1 were demonstrated to impact pharmacokinetics, or improve the drug resistance of pancreatic cancer, previously [41–43]. These variations of genetic expression in Mi-organoids further demonstrated their usability in building malignant tumor model *in vitro*.

3.5. Tumor chemosensitivity testing in PCOs

The morphology and size of 3D tumor tissue is crucial for the transportation of nutrient/oxygen, organization of spatial cellular structure and penetration/interaction of therapeutic agent [44,45]. As mentioned above, the Mi-organoids exhibited more uniform properties than Ma-organoids, which might affect their functions in biomedical applications, such as drug testing. To validate such hypothesis, we evaluated the responses of organoids to four anti-tumor drugs (Gemcitabine, Erlotinib, Olaparib, and 5-Fluorouracil) after 24 h of treatment. As shown in Fig. 6A, the relative viability of Mi-organoids cultured for 1 week before drug testing decreased in a dose-dependent manner, with varying effects for each drug. Specifically, the given organoids responded the most significantly to 5-Fluorouracil with only 38.05 % maintaining viability at the concentration of 1000 μM, while these organoids maintained 81.02 % viability when treated with Gemcitabine of 1000 μM. Generally, the PCOs can be generated for the drug screening after 2–4 weeks' culture [1], which has been decreased to 1 week for rapid screening in our system, though the microgels can support organoids culture for much longer. Since the PCOs within microgels were formed from single cells, which could partially replicate the tumor progression from the initial stage, the PCOs cultured for different duration in microgels might represent the different stage of pancreatic cancer. Thus, we tested the drug responses of PCOs that were cultured for 1 week or 2 weeks to investigate their differences. The results showed that PCOs cultured for 2 weeks before drug testing showed different responses to the same drug compared with that cultured for 1 week. For example, the killing effects of Erlotinib and 5-Fluorouracil were weakened for organoids cultured for 2 weeks, but such effects of Gemcitabine were strengthened.

Furthermore, we tested the drug responses of Mi-organoids and Ma-organoids to Erlotinib at a concentration of 50 μM that was supposed to significantly decrease the viability of organoids in this work. Erlotinib was added to the two organoids after 5 days of encapsulation, and these organoids were continuously treated for 5 days. As shown in Fig. 6B, cell viability of PCOs in microgels and Matrigel both deceased with treated time, while the Mi-organoids exhibited more concentrated data points compared with Ma-organoids at the same point. Thus, with Mi-organoids, accurate drug test results are expected to be obtained by doing less experiments, shortening the preclinical testing. From a different perspective, the experimental repeatability of Mi-organoids is better than that of Ma-organoids, confirmed by lower CV of cell viability (Fig. 6C), which further demonstrating the remarkable advantage of our strategy for improving organoid uniformity. In addition, we evaluated the proportion of cell proliferation and cell apoptosis in Mi-organoids cultured for 1 week after treatment with four drugs at different concentrations. The results showed that all these drugs led to the decrease of cell proliferation and increase of cell apoptosis in Mi-organoids (Fig. 6D-G), which was consistent with the variation of cell viability in Fig. 6A. Also, we evaluated the same data on Mi-organoids cultured for 2 weeks (Fig. S9). As a result, most of the PCOs responded to four drugs in similar trends in terms of the proportion of cell proliferation and cell apoptosis, whether cultured for one week or two weeks. However, the relative cell apoptosis of organoids treated with Gemcitabine and Olaparib for 24 h after 1 week and 2 weeks of culture exhibited remarkably differences, reflecting the weaker lethal effect of these drugs on tumor organoids with larger volume.

In addition, to evaluate the differences of molecular signatures of PCOs at different culture period, we analyzed the transcriptional profiles of organoids cultured for 1 week and 2 weeks by using RNA-seq. As shown in Fig. S10A, 174 genes are upregulated and 137 genes downregulated in Mi-organoids cultured for 2 weeks compared with that cultured for 1 week. All these genes were subjected to hierarchical clustering, showing the unique gene set enriched in organoids cultured for different periods (Fig. S10B). The selected KEGG pathway analysis was performed to estimate the mainly differentiated biological pathways between organoids cultured for 2 weeks and 1 week (Fig. S10C). The results showed that the biological pathways associated drug metabolism-cytochrome P450 was significantly upregulated in PCOs cultured for 2 weeks (Fig. S10D), which might account for the different responses of organoids to the same drug.

4. Discussion

Cancer organoids are promising alternatives in pathological research and drug screening of various tumors. In this study, we present a novel strategy for building PCOs with higher uniformity and controllability from single cells in a droplet system. The organoids are derived from single tumor cell in each microgel, resembling the original tumor clones in human bodies. The controllable initial state of seed cells and defined matrix enabled the uniform generation of PCOs. These organoids exhibit higher expression of the key biomarkers of pancreatic tumor and genes associated with drug metabolism. In addition, they have showed distinguishing responses to different clinical drugs in a reproducible manner.

In human body, a tumor is generally considered to originate from a normal cell, named as cell-of-origin, that has undergone tumorigenic transformation because of genetic mutations [46]. Although various theories, such as somatic, tissue organization field, bad luck, and ground state, have been proposed, all of these theories suggest that a tumor is derived from a single cell [47]. Currently, the patient-derived tumor organoids are generated from primary fragments or multi cells under 3D culture conditions [48], which cannot replicate the initial state of a tumor in the body. Thus, we provided a modified microfluidic approach to effectively encapsulate single tumor cell into isolated droplet, attempting to recapitulate the progression of tumor from the very beginning. Moreover, the controllable initial state of seed cells has improved the uniformity of PCOs in their size and morphology. Such approach has also significantly decreased the primary tissue amounts required for organoid formation, making it possible to build tumor organoids using biopsies from early detection of patients.

In addition, the existing tumor organoids are mostly seeded and manipulated manually [48], partially limit the throughput of organoid generation and automation of applications. In this work, the inherent advantage of droplet microfluidics in high-throughput fabrication has improved the efficiency of organoid establishment up to tens of thousands organoids per batch. In each batch, 80 %∼90 % of the single cells grew and self-assembled to form organoids with pancreatic cancer features. It is noteworthy that the micron-sized droplets or the synthetic microgels can be easily pipetted, transferred, and distributed using a commercial multichannel pipettor or automatic pipetting workstation, thereby enhancing flexibility and efficiency in organoid applications, such as drug screening.

Previous reports have demonstrated that tumor microenvironment (TME) played important roles in tumor progression, metastasis, vascularization, and therapy responses [49,50]. Especially, the stiffness of pancreatic cancer matrix is highly involved in tumor progression and phenotype, including their invasion [32], metastasis [33], fibrosis [34], and sensitivity to chemotherapy [16]. In this work, we tested the Young's modulus of commonly used Matrigel (0.17 kPa) in tumor organoid culture, which was remarkably lower than that of the primary tumor tissue (8.76 kPa). In addition, matrix like Matrigel exhibits high batch-to-batch variance, leading to a variable TME of PCOs. To address these issues, we developed microgels fabricated in the droplet system to serve as a controlled niche with appropriate stiffness, enabling the

growth and formation of tumor organoids from single cells. Organoids within these microgels maintained key biomarkers of pancreatic tumors and exhibited increased expression of relevant genes during culture. Moreover, unlike animal-derived matrices (e.g., Matrigel), these microgels consisted of a single component, CaA, with reduced variability. Also, the structural properties of microgels, including their size and aspect ratio, could be easily adjusted by modulating core flow rates and valve periods. Thus, each organoid formed within an isolated microgel was provided with a relatively consistent 3D microenvironment, instead of the multiple organoids cultured in different locations of the whole Matrigel matrix in the traditional system (Fig. 3A).

As a proof-of-concept, we tested the responses of Mi-organoids to several anti-cancer drugs after one or two weeks of culture. The results showed that Mi-organoids responded to all the four drugs positively, but exhibited distinct patterns in terms of cell viability, proliferation, and apoptosis. The new finding is that the uniform organoids can significantly improve the reproducibility and reliability of the drug testing results, which is not reported in previous studies. Furthermore, these organoids cultured for one or two weeks showed different responses to the same drug, which might be attributed to the differential expression of biological pathways associated with drug metabolism-cytochrome P450. Since the PCOs are derived from single cells, like the tumor progression *in vivo*, they hold the potential to be used for studying pancreatic cancer at different stages. Also, single cells can form obvious spheroids in the microgels within one week, and reliable data is expected to be obtained by doing less experiments with Mi-organoids, making this approach suitable for rapid drug screening for pancreatic cancer patients.

Inevitably, this study has a few limitations at present. Generally, PCOs were cultured within Matrigel or modified synthetic hydrogels that were biologically tuned. In this work, PCOs were cultured in alginate microgels without bioactive components, such as proteins. Actually, we tested several kinds of primary tumor cells and cells derived from stem cells using such microgels in our preliminary experiment, including mammary cancer cells, pancreatic cancer cells, endometrial cancer cells, intestinal cells, and nerve cells to investigate the formation of corresponding organoids. The results showed that some of these cells were not strictly dependent on bioactive components and formed the corresponding organoids, including mammary cancer organoids, PCOs and intestinal organoids, which was partially confirmed in the previous reports [51,52]. The alginate microgels successfully reproduced the mechanical properties of cancer matrix and provided 3D spatial support for the organoid formation, but they did not contain tumor-specific compositions, such as hyaluronic acid. This is not a fatal problem, as the commercial matrix, like Matrigel, cannot replicate the tumor-specific compositions, either. To further increase the quality of PCOs, the microgels are expected to be added tumor-specific components by modification with functional peptides or co-crosslinking with other defined polymers, without increasing their batch-to-batch variance. Additionally, the single cells are derived from patient tumor tissues which are inherently heterogenous, our approach can increase the apparent uniformity of tumor organoids at this stage to retain the richness of cell subtypes. More in-depth studies should be performed to explore the differences of the produced organoids from different single cells at gene and protein expression levels. Also, the comparation of tumor phenotypes between Mi-organoids and clinical biopsies are limited in this article. Such comparation can help us further understand the representativeness of Mi-organoids as *in vitro* tumor models. Since we focused more on presenting a novel way to generate uniform tumor organoids, and the possibility of utilizing them in drug testing, the existing data might already reflect our points. We are continuing our research to address these limitations.

5. Conclusion

In summary, we proposed a novel strategy for constructing uniform PCOs from single cells using a droplet system in a high-throughput manner, enabling the replication of tumor progression from the very beginning. Compared to existing protocols for establishing tumor organoids, this approach significantly reduces variation in the tumor niche and increases the uniformity of PCOs. Furthermore, the proposed approach integrates the formation, 3D cultures, and application of PCOs in a single system, which is comparable with commercial pipetting workstation for automated manipulations. We envision that the approach established in this work will contribute to advancing pathological studies and drug development for tumors in the future.

CRediT authorship contribution statement

Haitao Liu: Writing – review & editing, Writing – original draft, Methodology, Investigation, Funding acquisition, Conceptualization. **Tingting Tao:** Writing – review & editing, Writing – original draft, Methodology, Investigation, Funding acquisition, Conceptualization. **Zhongqiao Gan:** Methodology, Investigation. **Yingying Xie:** Visualization, Investigation. **Yaqing Wang:** Writing – review & editing, Visualization. **Yizhao Yang:** Writing – review & editing. **Xu Zhang:** Writing – review & editing, Funding acquisition. **Xianliang Li:** Supervision, Conceptualization. **Jianhua Qin:** Writing – review & editing, Writing – original draft, Supervision, Methodology, Conceptualization.

Data availability statement

The data that support the findings of this study are available from the corresponding authors upon reasonable request.

Declaration of competing interest

The authors declare no conflict of interest.

Acknowledgements

This research was supported by the National Key R&D Program of China (Nos. 2022YFA1205000, 2022YFA1104700, 2024YFA0919800), National Natural Science Foundation of China (Nos. 32171406, 32201184), Innovation Program of Science and Research from the DICP, CAS (No. DICP I202435), DMU-1&DICP (No. DMU-1&DICP UN202202).

Appendix A. Supplementary data

Supplementary data to this article can be found online at https://doi.org/10.1016/j.mtbio.2025.101765.

Data availability

Data will be made available on request.

References

[1] L.A. Baker, H. Tiriac, D.A. Tuveson, Generation and culture of human pancreatic ductal adenocarcinoma organoids from resected tumor specimens, Methods Mol. Biol. 1882 (2019) 97–115, https://doi.org/10.1007/978-1-4939-8879-2_9.
[2] I. Romero-Calvo, C.R. Weber, M. Ray, et al., Human organoids share structural and genetic features with primary pancreatic adenocarcinoma tumors, Mol. Cancer Res. 17 (2019) 70–83, https://doi.org/10.1158/1541-7786.mcr-18-0531.
[3] P.P. Praharaj, S.K. Bhutia, S. Nagrath, et al., Circulating tumor cell-derived organoids: current challenges and promises in medical research and precision medicine, BBA-Rev Cancer 1869 (2018) 117–127, https://doi.org/10.1016/j.bbcan.2017.12.005.
[4] M. Huch, H. Gehart, R. van Boxtel, et al., Long-term culture of genome-stable bipotent stem cells from adult human liver, Cell 160 (2015) 299–312, https://doi.org/10.1016/j.cell.2014.11.050.
[5] Z. Li, T. Araoka, J. Wu, et al., 3D culture supports long-term expansion of mouse and human nephrogenic progenitors, Cell Stem Cell 19 (2016) 516–529, https://doi.org/10.1016/j.stem.2016.07.016.

[6] M. van de Wetering, H.E. Francies, J.M. Francis, et al., Prospective derivation of a living organoid biobank of colorectal cancer patients, Cell 161 (2015) 933–945, https://doi.org/10.1016/j.cell.2015.03.053.

[7] E. Karzbrun, A. Kshirsagar, S.R. Cohen, et al., Human brain organoids on a chip reveal the physics of folding, Nat. Phys. 14 (2018) 515–522, https://doi.org/10.1038/s41567-018-0046-7.

[8] G. Vlachogiannis, S. Hedayat, A. Vatsiou, et al., Patient-derived organoids model treatment response of metastatic gastrointestinal cancers, Science 359 (2018) 920–926, https://doi.org/10.1126/science.aao2774.

[9] M. Simian, M.J. Bissell, Organoids: a historical perspective of thinking in three dimensions, J. Cell Biol. 216 (2017) 31–40, https://doi.org/10.1083/jcb.201610056.

[10] R.L. Siegel, K.D. Miller, N.S. Wagle, et al., Cancer statistics, 2023, CA Cancer J. Clin. 73 (2023) 17–48, https://doi.org/10.3322/caac.21763.

[11] M. Huch, P. Bonfanti, S.F. Boj, et al., Unlimited in vitro expansion of adult bi-potent pancreas progenitors through the Lgr5/R-spondin axis, EMBO J. 32 (2013) 2708–2721, https://doi.org/10.1038/emboj.2013.204.

[12] L.A. Baker, H. Tiriac, H. Clevers, et al., Modeling pancreatic cancer with organoids, Trends Cancer 2 (2016) 176–190, https://doi.org/10.1016/j.trecan.2016.03.004.

[13] E. Driehuis, A. van Hoeck, K. Moore, et al., Pancreatic cancer organoids recapitulate disease and allow personalized drug screening, Proc. Natl. Acad. Sci. U. S. A 116 (2019) 26580–26590, https://doi.org/10.1073/pnas.1911273116.

[14] Y.Q. Zhang, C.W. Houchen, M. Li, Patient-derived organoid pharmacotyping guides precision medicine for pancreatic cancer, Clin. Cancer Res. 28 (2022) 3176–3178, https://doi.org/10.1158/1078-0432.ccr-22-1083.

[15] E.A. Aisenbrey, W.L. Murphy, Synthetic alternatives to Matrigel, Nat. Rev. Mater. 5 (2020) 539–551, https://doi.org/10.1038/s41578-020-0199-8.

[16] A.J. Rice, E. Cortes, D. Lachowski, et al., Matrix stiffness induces epithelial-mesenchymal transition and promotes chemoresistance in pancreatic cancer cells, Oncogenesis 6 (2017), https://doi.org/10.1038/oncsis.2017.54.

[17] C.Y. Chang, C.C. Lin, Hydrogel models with stiffness gradients for interrogating pancreatic cancer cell fate, Bioengineering-Basel 8 (2021), https://doi.org/10.3390/bioengineering8030037.

[18] S. Ishihara, H. Haga, Matrix stiffness contributes to cancer progression by regulating transcription factors, Cancers 14 (2022), https://doi.org/10.3390/cancers14041049.

[19] S.W. Jiang, H.R. Zhao, W.J. Zhang, et al., An automated organoid platform with inter-organoid homogeneity and inter-patient heterogeneity, Cell Reports Medicine 1 (2020), https://doi.org/10.1016/j.xcrm.2020.100161.

[20] W.J. Zhang, D.H. Li, S.W. Jiang, et al., Microfluidic droplets as structural templates for Matrigel to enable 1-week large organoid modeling, Chem. Eng. Sci. 238 (2021), https://doi.org/10.1016/j.ces.2021.116632.

[21] S.L. Ding, C. Hsu, Z.H. Wang, et al., Patient-derived micro-organospheres enable clinical precision oncology, Cell Stem Cell 29 (2022) 905, https://doi.org/10.1016/j.stem.2022.04.006.

[22] G.S. Van Tienderen, J. Willemse, B. Van Loo, et al., Scalable production of size-controlled cholangiocyte and cholangiocarcinoma organoids within liver extracellular matrix-containing microcapsules, Cells 11 (2022), https://doi.org/10.3390/cells11223657.

[23] W.J. Zhang, H. Jin, S.T. Lou, et al., Microfluidic droplet encapsulation-guided organoid growth promotes parental tumor phenotype recapitulation, Int. J. Cancer (2023), https://doi.org/10.1002/ijc.34706.

[24] Y.M. Zhang, Q.F. Hu, Y.Q. Pei, et al., A patient-specific lung cancer assembloid model with heterogeneous tumor microenvironments, Nat. Commun. 15 (2024), https://doi.org/10.1038/s41467-024-47737-z.

[25] K.Y. Lee, D.J. Mooney, Alginate: properties and biomedical applications, Prog. Polym. Sci. 37 (2012) 106–126, https://doi.org/10.1016/j.progpolymsci.2011.06.003.

[26] B. Namgung, K. Ravi, P.P. Vikraman, et al., Engineered cell-laden alginate microparticles for 3D culture, Biochem. Soc. Trans. 49 (2021) 761–773, https://doi.org/10.1042/Bst20200673.

[27] A.S. Mao, J.W. Shin, S. Utech, et al., Deterministic encapsulation of single cells in thin tunable microgels for niche modelling and therapeutic delivery, Nat. Mater. 16 (2017) 236–243, https://doi.org/10.1038/nmat4781.

[28] X. Shi, Y. Li, Q. Yuan, et al., Integrated profiling of human pancreatic cancer organoids reveals chromatin accessibility features associated with drug sensitivity, Nat. Commun. 13 (2022) 2169, https://doi.org/10.1038/s41467-022-29857-6.

[29] H.T. Liu, H. Wang, W.B. Wei, et al., A microfluidic strategy for controllable generation of water-in-water droplets as biocompatible microcarriers, Small 14 (2018), https://doi.org/10.1002/smll.201801095.

[30] H.T. Liu, Y.Q. Wang, H. Wang, et al., A droplet microfluidic system to fabricate hybrid capsules enabling stem cell organoid engineering, Adv. Sci. 7 (2020), https://doi.org/10.1002/advs.201903739.

[31] D.M. Headen, G. Aubry, H. Lu, et al., Microfluidic-based generation of size-controlled, biofunctionalized synthetic polymer microgels for cell encapsulation, Adv Mater 26 (2014) 3003–3008, https://doi.org/10.1002/adma.201304880.

[32] A.V. Nguyen, K.D. Nyberg, M.B. Scott, et al., Stiffness of pancreatic cancer cells is associated with increased invasive potential, Integr. Biol. 8 (2016) 1232–1245, https://doi.org/10.1039/c6ib00135a.

[33] T.T. Chang, D. Thakar, V.M. Weaver, Force-dependent breaching of the basement membrane, Matrix Biol. 57–58 (2017) 178–189, https://doi.org/10.1016/j.matbio.2016.12.005.

[34] H.Y. Liu, T. Greene, T.Y. Lin, et al., Enzyme-mediated stiffening hydrogels for probing activation of pancreatic stellate cells, Acta Biomater. 48 (2017) 258–269, https://doi.org/10.1016/j.actbio.2016.10.027.

[35] X.F. Zheng, J.L. Carstens, J. Kim, et al., Epithelial-to-mesenchymal transition is dispensable for metastasis but induces chemoresistance in pancreatic cancer, Nature 527 (2015) 525, https://doi.org/10.1038/nature16064.

[36] Z.Y. Ma, Z.C. Li, Z.G. Ma, et al., Development of a KRAS-associated metabolic risk model for prognostic prediction in pancreatic cancer, Biomed Res Int (2021), https://doi.org/10.1155/2021/9949272, 2021.

[37] J.F. Zhang, J.Y. Gu, S.X. Guo, et al., Establishing and validating a pathway prognostic signature in pancreatic cancer based on miRNA and mRNA sets using GSVA, Aging-Us 12 (2020) 22840–22858.

[38] W. Xia, H.S. Bai, Y. Deng, et al., PLA2G16is a mutant p53/KLF5 transcriptional target and promotes glycolysis of pancreatic cancer, J. Cell Mol. Med. 24 (2020) 12642–12655, https://doi.org/10.1111/jcmm.15832.

[39] H. Ye, T.D. Li, H. Wang, et al., TSPAN1, TMPRSS4, SDR16C5, and CTSE as novel panel for pancreatic cancer: a bioinformatics analysis and experiments validation, Front. Immunol. 12 (2021), https://doi.org/10.3389/fimmu.2021.649551.

[40] K.Q. Hong, Q. Yang, H.S. Yin, et al., SDR16C5 promotes proliferation and migration and inhibits apoptosis in pancreatic cancer, Open Life Sci. 18 (2023), https://doi.org/10.1515/biol-2022-0630.

[41] K. Kattel, R. Evande, C. Tan, et al., Impact of CYP2C19 polymorphism on the pharmacokinetics of nelfinavir in patients with pancreatic cancer, Br. J. Clin. Pharmacol. 80 (2015) 267–275, https://doi.org/10.1111/bcp.12620.

[42] H.Q. Duong, K.S. You, S. Oh, et al., Silencing of NRF2 reduces the expression of ALDH1A1 and ALDH3A1 and sensitizes to 5-FU in pancreatic cancer cells, Antioxidants 6 (2017), https://doi.org/10.3390/antiox6030052.

[43] V.O. Oria, P. Bronsert, A.R. Thomsen, et al., Proteome profiling of primary pancreatic ductal adenocarcinomas undergoing additive chemoradiation link ALDH1A1 to early local recurrence and chemoradiation resistance, Transl Oncol 11 (2018) 1307–1322, https://doi.org/10.1016/j.tranon.2018.08.001.

[44] M. Singh, D.A. Close, S. Mukundan, et al., Production of uniform 3D microtumors in hydrogel microwell arrays for measurement of viability, morphology, and signaling pathway activation, Assay Drug Dev. Technol. 13 (2015) 570–583, https://doi.org/10.1089/adt.2015.662.

[45] O. Tartagni, A. Borók, E. Mensà, et al., Microstructured soft devices for the growth and analysis of populations of homogenous multicellular tumor spheroids, Cell. Mol. Life Sci. 80 (2023) 93, https://doi.org/10.1007/s00018-023-04748-1.

[46] K. Rycaj, D.G. Tang, Cell-of-Origin of cancer versus cancer stem cells: assays and interpretations, Cancer Res. 75 (2015) 4003–4011, https://doi.org/10.1158/0008-5472.Can-15-0798.

[47] A. Jassim, E.P. Rahrmann, B.D. Simons, et al., Cancers make their own luck: theories of cancer origins, Nat. Rev. Cancer 23 (2023) 710–724, https://doi.org/10.1038/s41568-023-00602-5.

[48] J. Drost, H. Clevers, Organoids in cancer research, Nat. Rev. Cancer 18 (2018) 407–418, https://doi.org/10.1038/s41568-018-0007-6.

[49] D.F. Quail, J.A. Joyce, Microenvironmental regulation of tumor progression and metastasis, Nat Med 19 (2013) 1423–1437, https://doi.org/10.1038/nm.3394.

[50] K.M. McAndrews, K.K. Mahadevan, R. Kalluri, Mouse models to evaluate the functional role of the tumor microenvironment in cancer progression and therapy responses, CSH Perspect Med 14 (2024) a041411, https://doi.org/10.1101/cshperspect.a041411.

[51] G.C. Fang, H.X. Lu, L.R. de la Fuente, et al., Mammary tumor organoid culture in non-adhesive alginate for luminal mechanics and high-throughput drug screening, Adv. Sci. 8 (2021), https://doi.org/10.1002/advs.202102418.

[52] M.M. Capeling, M. Czerwinski, S. Huang, et al., Nonadhesive alginate hydrogels support growth of pluripotent stem cell-derived intestinal organoids, Stem Cell Rep. 12 (2019) 381–394, https://doi.org/10.1016/j.stemcr.2018.12.001.